Modern Journal of Statistics
2(2), 30–56
DOI:https://doi.org/10.64389/mjs.2026.02268
https://sphinxsp.org/journal/index.php/mjs/

Research article

Novel DUS Topp-Leone Burr-Hatke exponential model with properties and application to COVID-19 datasets

U. F. Abbas[1], **O. D. Adubisi**[2,*]

[1] Department of Mathematics and Statistics, Gombe State Polytechnic, 762001 Bajoga, Nigeria; ufabbas@gspb.edu.ng

[2] Department of Statistics, Federal University Wukari, 670101 Wukari, Nigeria; adubisiobinna@fuwukari.edu.ng

* **Correspondence:** adubisiobinna@fuwukari.edu.ng

ARTICLE INFO

Keywords:
Burr-Hatke exponential model
COVID-19
DUS Topp-Leone family
Entropies
Maximum likelihood estimation

Mathematics Subject Classification:
60E05, 60F10, 62N05, 65C05

Important Dates:
Received: 13 January 2026
Revised: 12 April 2026
Accepted: 13 April 2026
Online: 15 April 2026

ABSTRACT

This study presents the DUSTopp-Leone Burr-Hatke-Exponential (DUSTL_{BHE}) model, a new and more flexible extension of the BHE model. The DUSTL_{BHE} model accommodates diverse density shapes such as right-skewed, heavy-tailed, unimodal, or decreasing, and failure rate patterns such as increasing, decreasing, inverted-bathtub, and reversed-J. Several statistical properties, including raw and incomplete moments, quantile and moment-generating functions, entropies, and order statistics, are derived and illustrated. The DUSTL_{BHE} model parameters are estimated using the maximum likelihood estimation (MLE) method. Simulation studies were utilized to assess the accuracy and efficiency of the MLE, while three real datasets from medical and engineering applications demonstrate the model's flexibility. The DUSTL_{BHE} model is compared with several competing distributions using standard goodness-of-fit criteria such as the log-likelihood, Akaike information criterion (AIC), Bayesian information criterion (BIC), corrected AIC (AICc), Hannan Quinn IC (HQIC), and Kolmogorov–Smirnov (KVS) statistics. The results show that the DUSTL_{BHE} distribution provides smaller AIC, BIC, AICc, HQIC, and KVS values and higher log-likelihood values than the competing models, indicating a superior fit to the datasets. These findings demonstrate that the DUSTL_{BHE} model is a flexible and useful alternative for modelling skewed and heavy-tailed real-world data, particularly in epidemiological and reliability studies.

1. Introduction

Classical distributions often fail to capture the characteristics of contemporary datasets, inspiring the development of new and more flexible distributional families. Researchers have therefore presented several generalizations of classical models to improve statistical inference and reliability in real-world applications. However, exact probability modeling is crucial in engineering and biomedical sciences, where inappropriate distributional selections can lead to unreliable inferences and stern consequences.

The Topp Leone (TL) family [47] and Burr Hatke (BH) family [26] of distributions have emerged as particularly influential in reliability and lifetime analysis. The TL family has generated several advanced variants, including power-TL-G family [40] , Transmuted TL-G family [50], New Power-TL Generated Family [17], exponentiated generalized TL-G family [39], TL discrete-Laplace distribution [5], Generalized TL-G family [44], TL-Kumaraswamy family [45], Tangent TL-G family [32], Cosine TL-G family [33], TL-Marshall-Olkin family [18], Alpha power generalized odd generalized exponential-G family [1], DUSTL-G family [20], TL-Kumaraswamy-Marshall-Olkin family [14], Lambert TL-G family [13], and others. The BH framework has produced many useful adaptations, such as exponentiated, logarithmic, unit, and weighted forms. These contributions demonstrate the growing importance of generalized distributions across reliability engineering, medical sciences, and applied statistics. This study builds on that progress by focusing on the Burr–Hatke Exponential (BHE) distribution, a one-parameter model introduced by [49]. Although the BHE has proven effective in diverse fields, its limited flexibility restricts its wider applicability. To address this, we propose an extended version of the BHE distribution, offering greater adaptability to various data structures.

Additionally, a persistent challenge lies in transforming complex and imprecise data into actionable insights that can enhance healthcare outcomes in medical science. Due to the intricate interplay of environmental, biological, and behavioral factors influencing human health, medical data are often difficult to interpret. Such data typically exhibit high dimensionality, noise, and uncertainty, making it challenging to derive precise conclusions [36]. To address these complexities, the use of probability distribution models has become increasingly essential. These provide a structured framework for quantifying and interpreting the inherent randomness in medical data, allowing researchers to extract meaningful and reliable information from otherwise unpredictable patterns.

The COVID-19 pandemic, in particular, has underscored the importance of probabilistic modelling in understanding and analysing global health crises. The stochastic nature of the pandemic, where outcomes depend on multiple interacting variables, has driven the need for innovative statistical techniques to model, interpret, and forecast its dynamics [6]. In response, numerous researchers have applied various probabilistic models to COVID-19 data, aiming to achieve better model fit, enhanced interpretability, and improved predictive accuracy in assessing the disease's spread and impact [15, 29, 21, 46, 34]. This study develops the mathematical properties of this novel model, explores the ability of the maximum likelihood estimation technique via simulation and demonstrates its utility through applications to COVID-19 and fibre strength datasets.

This study unfolds systematically across these sections. Section 2 presents the mathematical specification of the novel DUSTL-G family member. Section 3 develops linear representations and explores fundamental distributional properties of the DUSTL$_{BHE}$ model. Section 4 encompasses classical parameter estimation methodology with the maximum likelihood estimation (MLE) method . Section 5 simulation study is carried out to assess the accuracy and efficiency of the MLE, while Section 6 presents comprehen-

sive real-world data applications, followed by a conclusion in Section 7.

2. The Novel Distribution Genesis

The cumulative distribution function (cdf) of the BHE distribution introduced by [49] is specified as

$$G(y,\varphi) = 1 - \frac{e^{-\varphi y}}{1+\varphi y}, \quad y > 0, \varphi > 0, \tag{2.1}$$

and the probability density function (pdf) is specified as

$$g(y,\varphi) = \varphi e^{-\varphi y}\frac{2+\varphi y}{(1+\varphi y)^2}. \tag{2.2}$$

The cdf of the DUSTL-G family with a single shape parameter is introduced by [20] as

$$F(y;\eta,\xi) = \frac{e^{\left\{1-[1-G(y;\xi)]^2\right\}^{\eta}} - 1}{e-1}, \quad y > 0, \eta > 0, \tag{2.3}$$

and the pdf specified as

$$f(y;\eta,\xi) = \frac{2\eta g\{y;\xi\}[1-G(y;\xi)]\left\{1-[1-G(y;\xi)]^2\right\}^{\eta-1} e^{\left\{1-[1-G(y;\xi)]^2\right\}^{\eta}}}{e-1}. \tag{2.4}$$

where $e = \exp \approx 2.71828$. The baseline distribution vector of parameters ξ with cdf and pdf denoted as $G(y;\xi)$ and $g(y;\xi)$, respectively.

A random variable (r,v) Y follows the DUS-Topp Leone Burr Hatke Exponential (DUSTL_{BHE}) distribution with parameters $\eta > 0$ and $\varphi > 0$, denoted as $Y \sim \text{DUSTL}_{BHE}(\eta,\varphi)$, if its cdf by inserting Eq.(2.1) into Eq.(2.3) is specified as

$$F(y;\eta,\varphi) = \frac{e^{(1-u^2)^{\eta}} - 1}{e-1}, \quad y > 0, \tag{2.5}$$

with the first derivative of Eq.(2.5), the pdf specified as

$$f(y;\eta,\varphi) = \frac{2\varphi\eta(2+\varphi y)e^{-2\varphi y}}{(e-1)(1+\varphi y)^3}\left(1-u^2\right)^{\eta-1} e^{(1-u^2)^{\eta}}, \tag{2.6}$$

where $u = \frac{e^{-\varphi y}}{1+\varphi y}$.

The survival function $s(y;\eta,\varphi)$ and hazard rate function $h(y;\eta,\varphi)$ of the DUSTL_{BHE} distribution are specified, respectively as

$$S(y;\eta,\varphi) = \frac{e - e^{(1-u^2)^{\eta}}}{e-1}, \tag{2.7}$$

and

$$h(y;\eta,\varphi) = \frac{2\varphi\eta(2+\varphi y)e^{-2\varphi x}\left(1-u^2\right)^{\eta-1} e^{(1-u^2)^{\eta}}}{(1+\varphi y)^3\left[e - e^{(1-u^2)^{\eta}}\right]}. \tag{2.8}$$

The quantile function Q(p) is considered crucial for generating pseudo-random samples from the DUSTL$_{BHE}$ distribution. The Q(p) = F^{-1} (p) for $0 < p < 1$ is specified as

$$Q(p) = \frac{1}{\varphi}\left\{W\left(\frac{e}{\sqrt{K(p)}}\right) - 1\right\}, \tag{2.9}$$

where $K(p) = 1 - [\log(1 + p(e - 1))]^{1/\eta}$, W is the Lambert W function [19], e is the inverse of natural log function and u follows the uniform distribution. More so, the first, second (median), and third quantiles can be derived by inserting $u = 0.25$, $u = 0.5$, and $u = 0.75$ into Eq.(2.9), respectively.

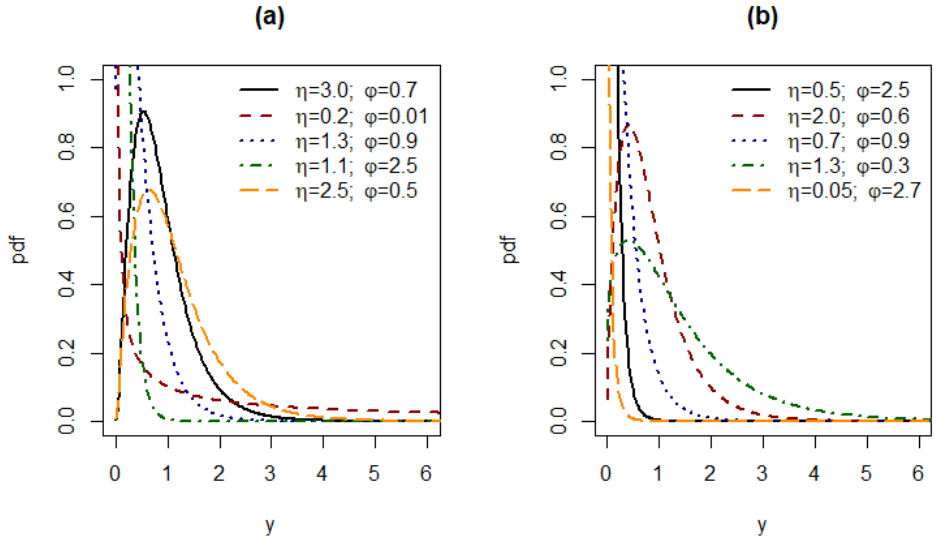

Figure 1. Density function plots for the DUSTL$_{BHE}$ model.

The motivation to introduce the DUSTL$_{BHE}$ is based on its flexibility with varying shapes such as right skewed, decreasing, and unimodal densities (see Figure 1). Moreover, the hazard rate function (hrf) has increasing-decreasing, increasing, inverted bathtub, decreasing, and reversed-J shaped ,making it more useful and an alternative to the baseline distribution (see Figures 2). Nonetheless, the novel DUSTL$_{BHE}$ distribution, which has two parameters, can also be extended with other families of distributions for greater flexibility and adaptability.

3. Linear representation and structural properties

3.1. Linear representation

Here, the linear representations of the cdf and pdf, useful for deriving the properties of the DUSTL$_{BHE}$ distribution, are presented. Firstly, applying the power series $(e^u - 1) = \sum_{i=1}^{\infty} \frac{u^i}{i!}$ and binomial series $(1 - u)^{\beta} = \sum_{j=0}^{\infty} (-1)^j \binom{\beta}{j} u^j$ for $|u| < 1$ [23, 2], to Eq.(2.5) leads to

$$F(y) = \sum_{i=1}^{\infty}\sum_{j=0}^{\infty} (-1)^j \binom{\eta i}{j} u^{2j}, \tag{3.1}$$

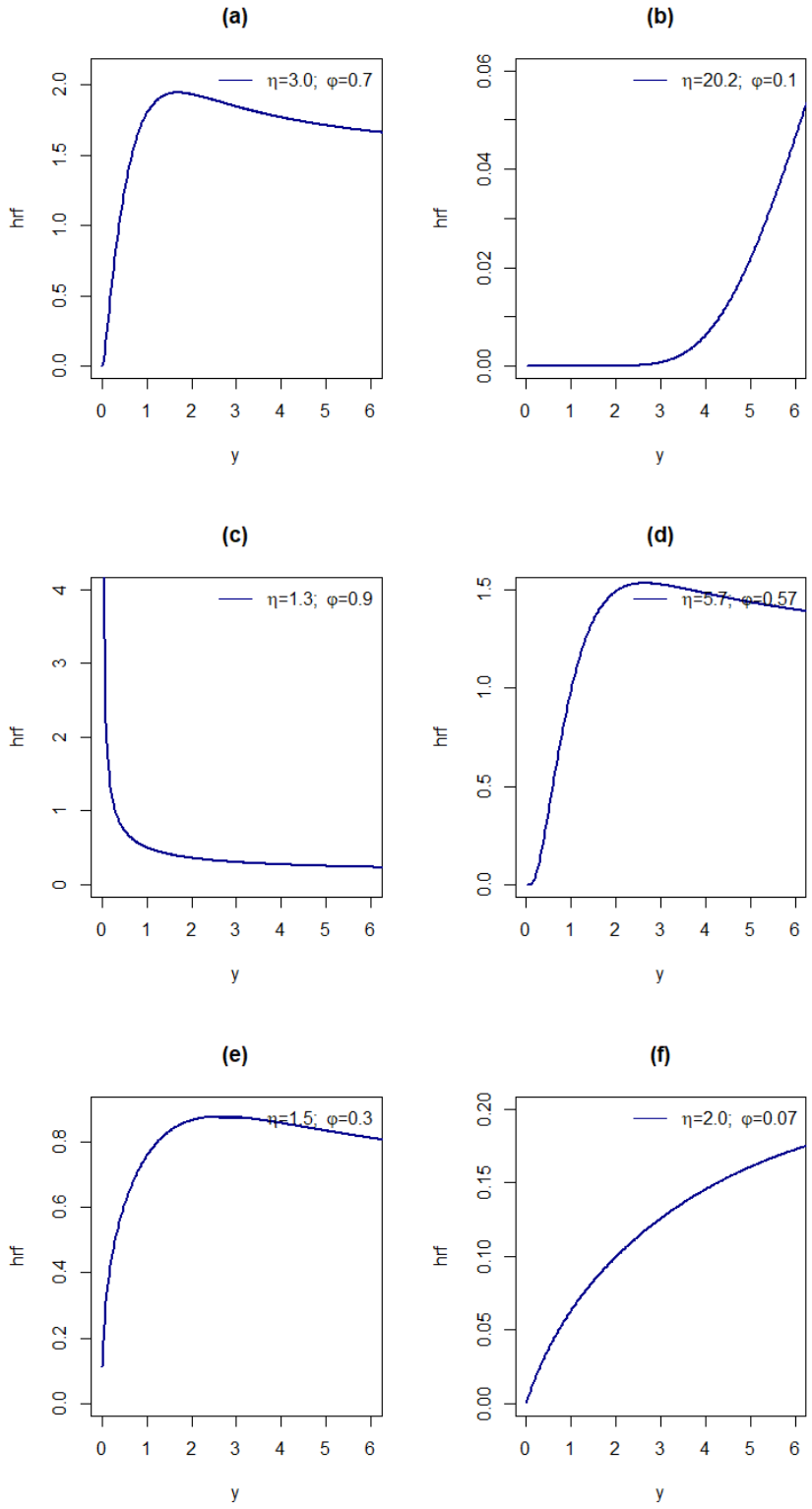

Figure 2. Hrf plots for the DUSTL$_{BHE}$ model.

where $u = \frac{e^{-\varphi y}}{1+\varphi y}$. Applying Taylor series expansion, $(1+z)^{-\beta} = \sum_{k=0}^{\infty}(-1)^k \binom{\beta+k-1}{k} z^k$ to Eq.(3.1), the linear form of the cdf is specified as

$$F(y) = \sum_{i=1}^{\infty} A_{j,k} y^k e^{-2j\varphi y}, \tag{3.2}$$

where $A_{j,k} = \sum_{j,k=0}^{\infty}(-1)^{j+k}\varphi^k \binom{\eta i}{j}\binom{2j+k-1}{k}$.

Correspondingly, applying power series $(e^u) = \sum_{j=0}^{\infty}\frac{u^j}{j!}$, binomial series and Taylor series expansions to Eq.(2.6) leads to

$$f(y) = 2\varphi\eta(2+\varphi y)\sum_{i=0}^{\infty}\sum_{j,k,l=0}^{\infty}(-1)^{i+k+l}\binom{\eta-1}{i}\binom{\eta j}{k}\binom{2(i+k+1)+l}{l}(\varphi y)^l e^{-2\varphi(i+k+1)y}, \tag{3.3}$$

Simplifying Eq.(3.3), the linear form of the pdf is specified as

$$f(y) = (2+\varphi y)\sum_{i=0}^{\infty} A^*_{j,k,l} y^l e^{-2\varphi(i+k+1)y}, \tag{3.4}$$

where $A^*_{j,k,l} = 2\eta\sum_{j,k,l=0}^{\infty}(-1)^{i+k+l}\varphi^{l+1}\binom{\eta-1}{i}\binom{\eta j}{k}\binom{2(i+k+1)+l}{l}$.

3.2. Structural Properties

Here, several statistical properties of the DUSTL$_{BHE}$ distribution are derived. These include the asymptotic behaviour, ordinary and incomplete moments, moment generating function, entropy and order statistic.

3.2.1. Asymptotic Properties

The asymptotic behaviour of the density, cumulative, and hazard rate functions of the DUSTL$_{BHE}$ distribution are presented in Table 1. The limiting behaviour of the provides insight into the behaviour of the model at the boundaries of the support. Specifically, the limits of the PDF, CDF, and hazard rate function were evaluated as $y \to 0^+$ and $y \to \infty$. These limits were obtained using the asymptotic properties of the exponential function and the structure of the Burr-Hatke exponential baseline distribution. As $y \to 0^+$, the exponential component approaches unity while the denominator term remains finite, resulting in a finite density value. This indicates that the proposed distribution assigns non-zero probability to observations near the origin. On the other hand, as $y \to \infty$, the exponential term tends to zero and consequently the density function approaches zero. This confirms that the proposed model has a light-tailed behaviour similar to exponential-type distributions. The limiting behaviour summarized in Table 1, therefore describes the boundary characteristics of the DUSTL$_{BHE}$ distribution and provides useful insight into its reliability and survival properties.

Table 1. Asymptotic behaviour of the DUSTL$_{BHE}$ distributions

Function	$y \to 0^+$	$y \to \infty$
$f(y)$	0	0
$F(y)$	0	1
$h(y)$	0	∞

3.2.2. Ordinary and Incomplete moments

The rth moment, say $\mu'_r = \int_0^\infty y^r f(y)\, dy$ for the DUSTL$_{BHE}$ using Eq.(3.4) can be derived as follows

$$\mu'_r = (2+\varphi y) \sum_{i=0}^{\infty} A^*_{j,k,l} \int_0^\infty y^{r+l} e^{-2\varphi(i+k+1)y} dy. \tag{3.5}$$

Simplifying Eq.(3.5) leads to

$$\mu'_r = \sum_{i=0}^{\infty} A^*_{j,k,l} \left[2 \int_0^\infty y^{r+l} e^{-2\varphi(i+k+1)y} dy + \varphi \int_0^\infty y^{r+l+1} e^{-2\varphi(i+k+1)y} dy \right]. \tag{3.6}$$

Let $z = 2\varphi(i+k+1)y \Rightarrow y = \frac{z}{2\varphi(i+k+1)}$ and $dy = \frac{dz}{2\varphi(i+k+1)}$, given that as $y \to 0 \Rightarrow z \to 0$ and $y \to \infty \Rightarrow z \to \infty$. Hence,

$$\mu'_r = \sum_{i=0}^{\infty} A^*_{j,k,l} \left\{ \frac{2}{[2\varphi(i+k+1)]^{r+l+1}} \int_0^\infty z^{r+l} e^{-z} dz + \frac{\varphi}{[2\varphi(i+k+1)]^{r+l+2}} \int_0^\infty z^{r+l+1} e^{-z} dz \right\}. \tag{3.7}$$

Utilizing the gamma integral form, say $\Gamma(\alpha) = \int_0^\infty z^{\alpha-1} e^{-z} dz$ with $\alpha - 1 = r + l$ and $\alpha = r + l + 1$ in Eq.(3.7) Therefore, the rth moment is specified as

$$\mu'_r = \sum_{i=0}^{\infty} A^*_{jkl} \left\{ \frac{2\Gamma(r+l+1)}{[2\varphi(i+k+1)]^{r+l+1}} + \frac{\varphi\Gamma(r+l+2)}{[2\varphi(i+k+1)]^{r+l+2}} \right\}, \tag{3.8}$$

where $\Gamma(\cdot)$ is the gamma function. The first four moments are derived by inserting $r = 1, 2, 3, 4$ into Eq.(3.8). The mean expression with $r = 1$ for the DUSTL$_{BHE}$ distribution is specified as

$$\mu'_1 = \sum_{i=0}^{\infty} A^*_{jkl} \left\{ \frac{2\Gamma(l+2)}{[2\varphi(i+k+1)]^{l+2}} + \frac{\varphi\Gamma(l+3)}{[2\varphi(i+k+1)]^{l+3}} \right\}. \tag{3.9}$$

Table 2 presents the numerical values of first four moments, Skewness (SK), Kurtosis (KU), standard deviation (SD), coefficient of variation (CV), and dispersion index (DI) for different parameter combinations of the DUSTL$_{BHE}$ distribution. The DI less than one for all the parameter combinations indicate under dispersion . Also, the CV $>$ 20% suggests that the new distribution can handle datasets that are more spread out relative to the mean. Also, the results show that the skewness varies from 1.64 to 2.63, indicating that the distribution remains positively skewed for all parameter configurations considered. The increase in skewness occurs because the shape parameter (η) controls the asymmetry and tail behaviour of the distribution. When the shape parameter (η) increases while the scale parameter (φ) remains moderate, the right tail becomes longer and heavier, thereby increasing the skewness coefficient.

Furthermore, the kurtosis values demonstrate the ability of the proposed model to capture heavy-tailed behaviour. In particular, the kurtosis value of 13.94 observed for one parameter combination indicates a highly leptokurtic distribution. Such large kurtosis arises when the probability mass becomes concentrated near the central region, while extreme observations occur with relatively higher probability in the right tail. This behaviour highlights the flexibility of the DUSTL$_{BHE}$ distribution in modelling datasets that exhibit strong skewness and heavy-tailed characteristics.

Figure 3 depicts the 3-D plots of the statistical properties of the DUSTL$_{BHE}$ model with varied values of η and φ. The plots support the results presented in Table 2 for the various statistical measures.

Table 2. Descriptive measures of the DUSTL$_{BHE}$ model

μ'_r	(1.5, 0.5)	(2.5, 1.5)	(0.5, 1.5)	(0.9, 2.5)
μ'_1	0.8863	0.3804	0.1510	0.1327
μ'_2	1.3226	0.2142	0.0594	0.0352
μ'_3	2.8542	0.1646	0.0385	0.0144
μ'_4	8.2649	0.1645	0.0354	0.0081
SK	1.8538	1.6464	2.6320	2.1481
KU	8.7653	7.6952	13.9430	10.5053
SD	0.7329	0.2637	0.1914	0.1328
CV	0.8269	0.6932	1.2680	1.0011
DI	0.6061	0.1828	0.2427	0.1330

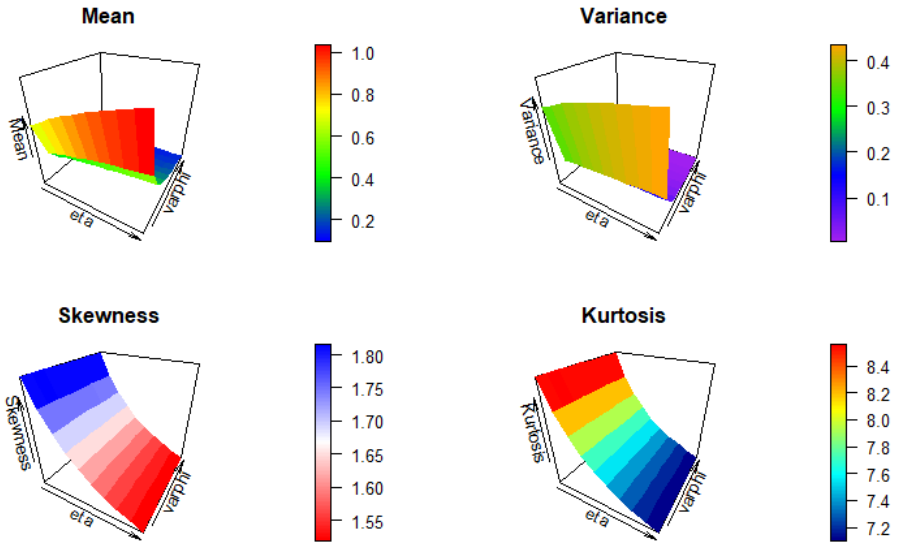

Figure 3. The Mean, Variance, Skewness, and Kurtosis plots for the DUSTL$_{BHE}$ distribution.

Likewise, the incomplete moment (IM) , say $I_r(t) = \int_0^t y^r f(y)\, dy$ for the DUSTL$_{BHE}$ is specified as

$$I_r(t) = \sum_{i=0}^{\infty} A^*_{j,k,l} \left[2 \int_0^t y^{r+l} e^{-2\varphi(i+k+1)y} dy + \varphi \int_0^t y^{r+l+1} e^{-2\varphi(i+k+1)y} dy \right]. \tag{3.10}$$

Let $z = 2\varphi(i+k+1)y \Rightarrow y = \frac{z}{2\varphi(i+k+1)}$ and $dy = \frac{dz}{2\varphi(i+k+1)}$, given that as $y \to 0 \Rightarrow z \to 0$ and $y \to t \Rightarrow z \to 2\varphi(i+k+1)t$.

Utilising the incomplete gamma integral form, say $\gamma(\alpha, t) = \int_0^t z^{\alpha-1}e^{-z}dz$, and following the same part that led to Eq.(3.8) on Eq.(3.10). The IM is specified as

$$I_r(t) = \sum_{i=0}^{\infty} A^*_{jkl}\left\{\frac{2\gamma[r+l+1, 2\varphi(i+k+1)t]}{[2\varphi(i+k+1)]^{r+l+1}} + \frac{\varphi\gamma[r+l+2, 2\varphi(i+k+1)t]}{[2\varphi(i+k+1)]^{r+l+2}}\right\}, \tag{3.11}$$

where $\gamma(\cdot)$ is the incomplete gamma function. The first incomplete moment of the DUSTL$_{BHE}$ distribution is derived by inserting $r = 1$ into Eq.(3.11).

3.2.3. Moment generating function

The moment generating function (MGF) of the DUSTL$_{BHE}$ distribution, say $M_X(t)$ is

$$M_Y(t) = \mathrm{E}\left(e^{tY}\right) = \sum_{r=0}^{\infty}\frac{t^r}{r!}\int_0^{\infty} y^r f(y)\,dy = \sum_{r=0}^{\infty}\frac{t^r}{r!}\mu'_r. \tag{3.12}$$

By inserting Eq. (3.8) into Eq. (3.12), the MGF is specified as

$$M_Y(t) = \sum_{r=0}^{\infty}\sum_{i=0}^{\infty}\frac{A^*_{jkl}t^r}{r!}\left\{\frac{2\Gamma(r+l+1)}{[2\varphi(i+k+1)]^{r+l+1}} + \frac{\varphi\Gamma(r+l+2)}{[2\varphi(i+k+1)]^{r+l+2}}\right\}. \tag{3.13}$$

3.2.4. Entropy

Entropy measures serve as fundamental tools for quantifying variability and uncertainty within systems. This study utilizes the Shannon entropy [42], Rényi entropy [38], Havrda-Charvat entropy [25], Arimoto entropy [11], and Tsallis entropy [48] to assess the degree of randomness present in the r.v. of the DUSTL$_{BHE}$ distribution. The Rényi entropy is defined as

$$R_{(y)}(\lambda) = \frac{1}{1-\lambda}\log\int_0^{\infty} f^{\lambda}(y)\,dy,\ \ \lambda > 0 \text{ and } \lambda \neq 1, \tag{3.14}$$

inserting Eq. (2.6) into Eq. (3.14)

$$R_{(y)}(\lambda) = \frac{1}{1-\lambda}\log\int_0^{\infty}\left(\frac{2\varphi\eta(2+\varphi y)e^{-2\varphi y}}{(e-1)(1+\varphi y)^3}\left(1-u^2\right)^{\eta-1}e^{(1-u^2)^{\eta}}\right)^{\lambda}dx, \tag{3.15}$$

where $u = \frac{e^{-\varphi y}}{1+\varphi y}$, then following the same paths that led to Eq. (3.8), the Rényi entropy of the DUSTL$_{BHE}$ distribution is specified as

$$R_{(y)}(\lambda) = \frac{1}{1-\lambda}\log\left(\sum_{i=0}^{\infty}A^{**}_{jkl}\left\{\frac{2^{\lambda}\Gamma(l+1)}{[2\varphi(i+k+\lambda)]^{l+1}} + \frac{\varphi^{\lambda}\Gamma(l+\lambda+1)}{[2\varphi(i+k+\lambda)]^{l+\lambda+1}}\right\}\right), \tag{3.16}$$

where $A^{**}_{j,k,l} = (2\eta)^{\lambda}\sum_{j,k,l=0}^{\infty}(-1)^{i+k+l}\varphi^{l+\lambda}\binom{\lambda(\eta-1)}{i}\binom{\eta j}{k}\binom{2(i+k)+3\lambda+l-1}{l}$.

Likewise, the Tsallis entropy defined as $T_{(y)}(\lambda) = \frac{1}{\lambda-1}\log\left[1-\int_0^{\infty}f^{\lambda}(y)\,dy\right], \lambda \neq 1, \lambda > 0$ is considered for the DUSTL$_{BHE}$ distribution and specified as

$$T_{(y)}(\lambda) = \frac{1}{\lambda - 1} \log \left[1 - \left(\sum_{i=0}^{\infty} A_{jkl}^{**} \left\{ \frac{2^{\lambda} \Gamma(l+1)}{[2\varphi(i+k+\lambda)]^{l+1}} + \frac{\varphi^{\lambda} \Gamma(l+\lambda+1)}{[2\varphi(i+k+\lambda)]^{l+\lambda+1}} \right\} \right) \right]. \tag{3.17}$$

The Arimoto entropy defined as $A_{(y)}(\lambda) = \frac{\lambda}{1-\lambda} \left\{ \left[\int_0^{\infty} f^{\lambda}(x)\, dx \right]^{\frac{1}{\lambda}} - 1 \right\}, \lambda \neq 1, \lambda > 0$ is considered for the DUSTL$_{BHE}$ distribution and specified as

$$A_{(y)}(\lambda) = \frac{\lambda}{1 - \lambda} \left[\left(\sum_{i=0}^{\infty} A_{jkl}^{**} \left\{ \frac{2^{\lambda} \Gamma(l+1)}{[2\varphi(i+k+\lambda)]^{l+1}} + \frac{\varphi^{\lambda} \Gamma(l+\lambda+1)}{[2\varphi(i+k+\lambda)]^{l+\lambda+1}} \right\} \right)^{\frac{1}{\lambda}} - 1 \right]. \tag{3.18}$$

The Havrda-Charvat entropy defined as $HC_{(y)}(\lambda) = \frac{1}{2^{(1-\lambda)}-1} \left\{ \left[\int_0^{\infty} f^{\lambda}(y)\, dy \right] - 1 \right\}$ is considered for the DUSTL$_{BHE}$ distribution and specified as

$$HC_{(y)}(\lambda) = \frac{1}{2^{(1-\lambda)} - 1} \left[\left(\sum_{i=0}^{\infty} A_{jkl}^{**} \left\{ \frac{2^{\lambda} \Gamma(l+1)}{[2\varphi(i+k+\lambda)]^{l+1}} + \frac{\varphi^{\lambda} \Gamma(l+\lambda+1)}{[2\varphi(i+k+\lambda)]^{l+\lambda+1}} \right\} \right) - 1 \right], \tag{3.19}$$

where $\Gamma(\cdot)$ is the gamma function. The Shannon entropy, say $S_{(y)}(1) = E\{-[\log f(y)]\}$ is a special case of the other entropies as $\lambda \to 1$. Table 3 reports the estimates of the entropies for various order (λ) and parameter values of the DUSTL$_{BHE}$ distribution.

Figure 4 depicts the graphical forms of the degree of randomness based on each entropy for the DUSTL$_{BHE}$ model with fixed values of η and φ. The plots support the results presented in Table 3, which shows that the degree of uncertainty decreases as the order of entropy increases for the DUSTL$_{BHE}$ distribution.

Table 3. Entropies estimates for the DUSTL$_{\text{BHE}}$ distribution.

η	φ	λ	$S_{(y)}(1)$	$R_{(y)}(\lambda)$	$T_{(y)}(\lambda)$	$A_{(y)}(\lambda)$	$HC_{(y)}(\lambda)$
1.5	1.0	0.5	0.138657	0.46305	0.52104	0.58900	0.62895
		0.8	0.138657	0.23063	0.23603	0.23700	0.31747
		1.2	0.138657	0.07150	0.07099	0.07100	0.10968
		1.5	0.138657	-0.00175	-0.00175	-0.00200	-0.00299
		2.0	0.138657	-0.08316	-0.08671	-0.08500	-0.17342
2.0	0.5	0.5	0.925189	1.22949	1.69837	2.41900	2.05012
		0.8	0.925189	1.01139	1.12095	1.15100	1.50768
		1.2	0.925189	0.86216	0.79193	0.80300	1.22353
		1.5	0.925189	0.79325	0.65483	0.69700	1.11786
		2.0	0.925189	0.71631	0.51145	0.60200	1.02289
1.0	2.0	0.5	-0.736714	-0.35818	-0.32794	-0.30100	-0.39586
		0.8	-0.736714	-0.62725	-0.58950	-0.58100	-0.79288
		1.2	-0.736714	-0.81788	-0.88858	-0.87600	-1.37286
		1.5	-0.736714	-0.90770	-1.14873	-1.06000	-1.96100
		2.0	-0.736714	-1.00920	-1.74341	-1.31300	-3.48683

Table 3 reports the Shannon, Rényi, Tsallis, Arimoto, and Havrda Charvat entropy measures of the DUSTL$_{BHE}$ distribution for selected parameter values. It is worth noting that the Shannon entropy values

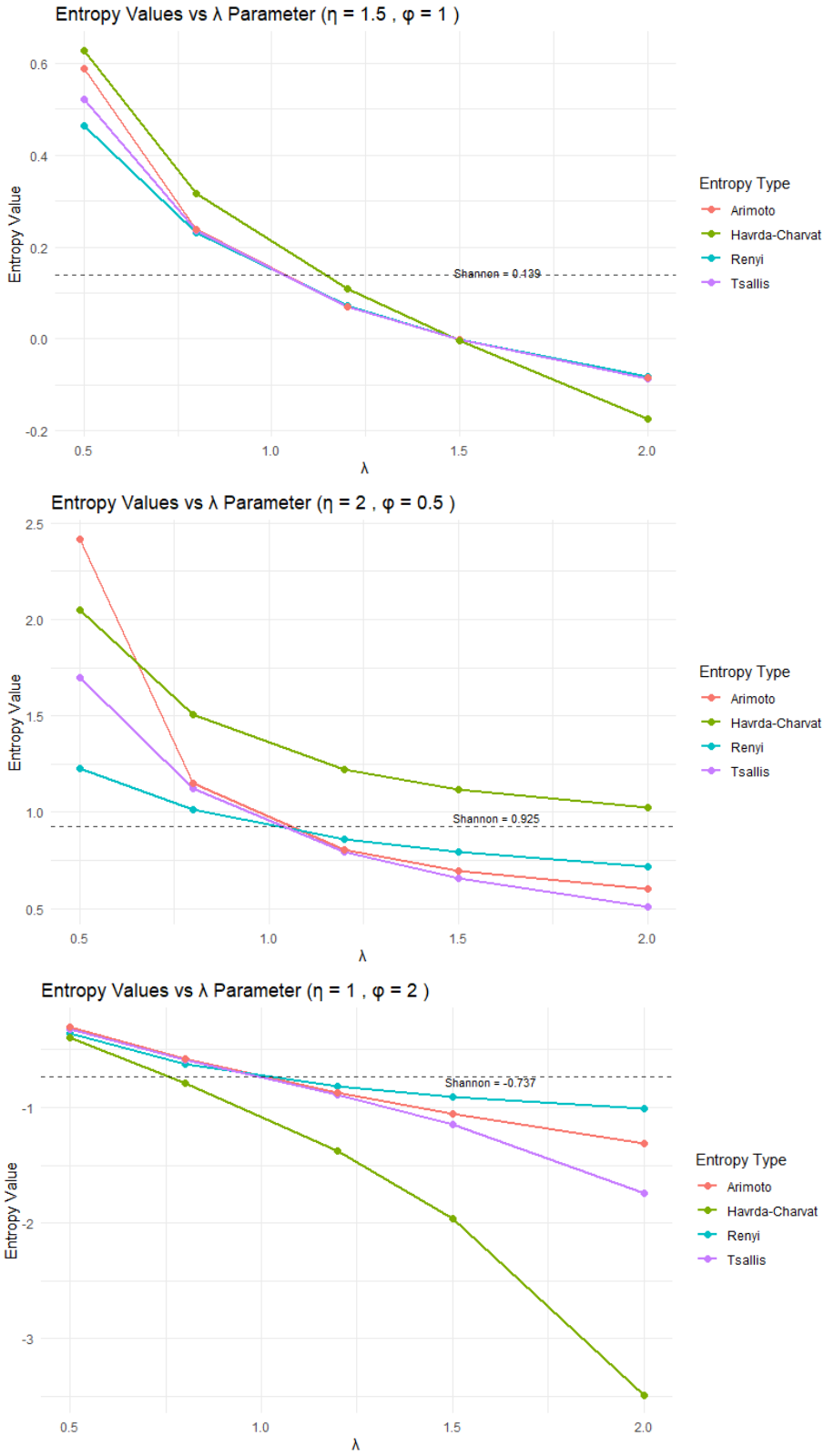

Figure 4. Entropies plots for the DUSTL$_{BHE}$ distribution.

can be negative because the entropy computed here corresponds to the differential entropy of a continuous distribution. Unlike discrete entropy, differential entropy may take negative values when the probability density function is highly concentrated around certain regions of the support. Thus, the negative entropy values observed indicate that the distribution becomes highly concentrated, implying lower uncertainty in the random variable.

The results further show that the Rényi entropy decreases as the parameter λ increases. This behaviour occurs because larger values of λ increase the decay rate of the distribution, which concentrates probability mass closer to the origin. As a result, the variability and uncertainty of the distribution decrease. Therefore, the decreasing pattern of Rényi entropy suggests that larger values of λ correspond to more predictable outcomes, whereas smaller values allow greater dispersion and uncertainty in the distribution.

3.2.5. Order Statistics

If $y_1, y_2, \ldots, y_n$ be a random sample from the DUSTL$_{BHE}$ r.v with $x_{p:n}$ as the order statistics (O.S). The pdf of the p$^{\text{th}}$ O.S, say $f_{p:n}(y)$ is expressed as

$$f_{p:n}(y) = \frac{1}{B(p, n-p+1)} g(y) [G(y)]^{p-1} [1 - G(y)]^{n-p}, \tag{3.20}$$

by expanding the last part of Eq. (3.20) using the binomial series expansion $(1-u)^{\beta} = \sum_{j=0}^{\infty} (-1)^j \binom{\beta}{j} u^j$ for $|u| < 1$, the pdf of the p$^{\text{th}}$ O.S is given by

$$f_{p:n}(y) = \frac{1}{B(p, n-p+1)} \sum_{i=0}^{n-p} (-1)^i \binom{n-p}{i} [G(y)]^{p+i-1} g(y), \tag{3.21}$$

inserting Eqs. (2.5) and (2.6) into Eq. (3.21), we have

$$\begin{aligned} f_{p:n}(y) = \tfrac{1}{B(p,n-p+1)} \textstyle\sum_{i=0}^{n-p} (-1)^i \binom{n-p}{i} \left[\tfrac{e^{(1-u^2)^{\eta}}-1}{e-1}\right]^{p+i-1} \\ \times \tfrac{2\varphi\eta(2+\varphi y)e^{-2\varphi y}}{(e-1)(1+\varphi y)^3} \left(1-u^2\right)^{\eta-1} e^{(1-u^2)^{\eta}}. \end{aligned} \tag{3.22}$$

Then, applying the power series $(e^u - 1) = \sum_{i=1}^{\infty} \frac{u^i}{i!}$ and binomial series $(1-u)^{\beta} = \sum_{j=0}^{\infty} (-1)^j \binom{\beta}{j} u^j$ for $|u| < 1$ expansions to Eq.(3.22). The p$^{\text{th}}$ O.S is specified as

$$f_{p:n}(y) = \frac{(2+\varphi y)}{B(p, n-p+1)} \sum_{i=0}^{n-p} A^{***}_{i,j,k,n,m,g} y^g e^{-2\varphi(m+n+1)y}, \tag{3.23}$$

where $B(\cdot)$ is the beta function and

$$\begin{aligned} A^{***}_{i,j,k,n,m,g} = 2\eta \textstyle\sum_{i,j,k,n,m,g=0}^{\infty} \tfrac{(-1)^{i+j+n+m+g}(j+1)^k \varphi^{g+1}}{k!(e-1)^{p+i}} \binom{n-p}{i} \binom{p+i-1}{j} \binom{\eta k}{n} \\ \times \binom{\eta-1}{m} \binom{m+n+2+g}{g}. \end{aligned}$$

Inserting $p = 1$ and $p = n$ in Eq. (3.23), the minimum and maximum order statistics of the DUSTL$_{BHE}$ distribution are derived, respectively.

4. Estimation for complete samples

Here, the estimator for the DUSTL$_{BHE}$ parameters using uncensored datasets is presented. Let $y_1, y_2, \ldots, y_n$ be the random observed values of size (n) from DUSTL$_{BHE}(\eta, \varphi)$, the ML estimates (MLE) are obtained from the log-likelihood function of Eq. (2.6), specified as

$$\begin{aligned}\ell(\eta,\varphi) = n\ln(2\varphi\eta) - n\ln(\exp -1) + \textstyle\sum_{i=1}^{n}\ln(2+\varphi y_i) - 3\sum_{i=1}^{n}\ln(1+\varphi y_i) - 2\varphi\sum_{i=1}^{n} y_i \\ +(\eta-1)\textstyle\sum_{i=1}^{n}\ln(1-u_i^2) + \sum_{i=1}^{n}[1-u_i^2]^{\eta},\end{aligned} \tag{4.1}$$

where $u_i = \frac{\exp(-\varphi y_i)}{1+\varphi y_i}$.
The partial derivative of Eq. (4.1) with respect to η and φ are given as

$$\frac{\partial \ell}{\partial \eta} = \frac{n}{\eta} + \sum_{i=1}^{n}\ln\left(1-u_i^2\right)\left[1+\left(1-u_i^2\right)^{\eta}\right], \tag{4.2}$$

and

$$\begin{aligned}\frac{\partial \ell}{\partial \varphi} = \frac{n}{\varphi} + \textstyle\sum_{i=1}^{n}\frac{y_i}{2+\varphi y_i} - 3\sum_{i=1}^{n}\frac{y_i}{1+\varphi y_i} - 2\sum_{i=1}^{n} y_i + 2(\eta-1)\sum_{i=1}^{n}\frac{u_i y_i \exp(-\varphi y_i)(2+\varphi y_i)}{(1-u_i^2)(1+\varphi y_i)^2} \\ +2\eta\textstyle\sum_{i=1}^{n}\frac{(1-u_i^2)^{\eta-1}u_i y_i \exp(-\varphi y_i)(2+\varphi y_i)}{(1+\varphi y_i)^2}\ .\end{aligned} \tag{4.3}$$

The ML estimates $\hat{\eta}_{\mathrm{ML}}$ and $\hat{\varphi}_{\mathrm{ML}}$ can be found by solving the non-linear functions simultaneously by equating Eqs. (4.2) and (4.3) to zero.

5. Simulation

Here, a simulation study is utilized to assess the accuracy and efficiency of the MLE in estimating the parameters (pa) of the DUSTL$_{BHE}$ distribution. The simulation is carried out as follows:

1. Data are generated using the quantile function in Eq. (2.9).

$$y = \frac{1}{\varphi}\left\{W\left(\frac{e}{\sqrt{K(p)}}\right) - 1\right\},$$

   where $K(p) = 1 - [\log(1 + p(e-1))]^{1/\eta}$.
2. The initial parameter combinations are: $(\eta = 0.5, \varphi = 0.7)$, $(\eta = 1.5, \varphi = 0.9)$, $(\eta = 2.0, \varphi = 1.5)$ and $(\eta = 1.0, \varphi = 2.0)$.
3. The designated sample sizes are $n = 25, 75, 150$ and 250.
4. Generate 10,000 replicates for each sample size.

The performance is evaluated through the average estimates (AVEs), bias, and root mean square errors (RMSEs) for the different sample sizes. The bias and RMSE are computed for $\hat{\Phi} = \hat{\eta}, \hat{\varphi}$, using

$$\hat{Bias} = \frac{1}{10000}\sum_{i=1}^{10000}\left(\hat{\Phi}_i - \Phi\right),$$

$$\hat{RMSE} = \sqrt{\frac{1}{10000}\sum_{i=1}^{10000}\left(\hat{\Phi}_i - \Phi\right)^2}.$$

The numerical results presented in Table 4 , show that the bias and RMSE decreases as the sample size increases for each initial parameter combination. This shows the consistency property of the MLEs.

6. Applicability to Real-World Datasets

This section presents the practical demonstration of the novel DUSTL$_{BHE}$ distribution in modeling real-world datasets. The performance validation is achieved by analysing three actual datasets to establish its superiority in comparison to several existing distributions, namely Topp-Leone Burr Hatke exponential (TLBHE) by [10], alpha power exponential (APE) by [31], Burr Hatke exponential (BHE) by [49], alpha power Burr Hatke (APBH) by [4], Burr Hatke (BH) by [26], Pareto (PE) by [27], inverse Pareto (IPE) by [28], Pareto type-I (PE1) by [12], Gompertz (GOM) by [22], Exponentiated Inverse Rayleigh (EIR) by [37], Lomax (LOMX) by [30] and exponential (E) by [16] distributions utilizing the *AdequacyModel* package in R-program software.

For the three datasets, the following performance measures are computed and utilized in selecting the best performing distribution: negative log-likelihood ($-\ell$), Akaike information criteria (AIC), corrected AIC (cAIC), Bayesian IC (BIC), Hannan Quinn IC (HQIC), Anderson–Darling (ANDL), Cramér–von Mises (CVMS), and Kolmogorov–Smirnov (KSV) with corresponding p-value (KSPV).

The first real dataset concerns the daily number of confirmed deaths attributed to COVID-19, taken from the Saudi Ministry of Health, reported by [8]. The recorded observations are as follows: 1.00, 1.00, 2.00, 4.00, 5.00, 1.00, 1.00, 3.00, 6.00, 6.00, 4.00, 1.00, 5.00, 6.00, 6.00, 8.00, 5.00, 7.00, 7.00, 9.00, 9.00, 15.00, 17.00, 11.00, 13.00, 5.00, 14.00, 5.00, 13.00, 9.00, 19.00, 15.00, 11.00, 14.00, 12.00, 11.00, 7.00, 13.00, 10.00, 20.00, 22.00, 21.00, 12.00, 14.00, 9.00, 14.00, 7.00, 16.00, 17.00, 13.00, 21.00, 11.00, 11.00, 8.00, 11.00, 12.00, 15.00, 21.00, 20.00, 18.00, 15.00, 14.00, 21.00, 16.00, 11.00, 28.00, 29.00, 19.00, 14.00, 19.00, 29.00, 34.00, 34.00, 46.00, 46.00, 47.00, 36.00, 38.00, 40.00, 32.00, 39.00, 34.00, 35.00, 36.00, 35.00, 45.00, 62.00. This dataset has been utilized to assess the performance of statistical models in capturing the variability and distributional characteristics of pandemic-related mortality data. See, [9], [24]. Figures 5 depict the dataset features using the Box-plot, TTT plot, kernel-density plot, and strip plot. The plots confirm presents of outliers, right-skewness and increasing failure rate.

Table 5 presents the MLEs with standard errors (SEs) and performance measures for the novel DUSTL$_{BHE}$ and the competing distributions. The novel DUSTL$_{BHE}$ has the least values for the performance measures, especially the KSV with high KSPV, confirming the model offers the best fit to the first dataset. Figure 6 depicts clear evidence that the novel DUSTL$_{BHE}$ offers the best fit through the empirical pdf with histogram, empirical cdf, empirical survival, probability-propability (P-P), and quantile-quantile (Q-Q) plots. Figure 7 depicts the log-likelihood profile plots with the estimated MLE parameter values for the first dataset. Furthermore, the empirical findings indicate that the novel model fits the first dataset

Table 4. Simulation results for $\text{DUSTL}_{\text{BHE}}$ distribution.

n	Pa	AVE	Bias	RMSE
		$(\eta = 0.5, \varphi = 0.7)$		
25	η	0.566	0.066	0.196
	φ	0.797	0.097	0.286
75	η	0.521	0.021	0.089
	φ	0.731	0.031	0.139
150	η	0.510	0.010	0.060
	φ	0.714	0.014	0.093
250	η	0.506	0.006	0.046
	φ	0.708	0.008	0.071
		$(\eta = 1.5, \varphi = 0.9)$		
25	η	1.806	0.306	0.863
	φ	0.989	0.089	0.273
75	η	1.590	0.090	0.339
	φ	0.929	0.029	0.138
150	η	1.543	0.043	0.222
	φ	0.913	0.013	0.094
250	η	1.525	0.025	0.168
	φ	0.908	0.008	0.072
		$(\eta = 2.0, \varphi = 1.5)$		
25	η	2.463	0.463	1.309
	φ	1.641	0.141	0.434
75	η	2.134	0.134	0.487
	φ	1.546	0.046	0.220
150	η	2.064	0.064	0.317
	φ	1.521	0.021	0.149
250	η	2.036	0.036	0.238
	φ	1.512	0.012	0.114
		$(\eta = 1.0, \varphi = 2.0)$		
25	η	1.172	0.172	0.491
	φ	2.217	0.217	0.662
75	η	1.052	0.052	0.205
	φ	2.071	0.071	0.332
150	η	1.025	0.025	0.136
	φ	2.033	0.033	0.225
250	η	1.014	0.014	0.103
	φ	2.019	0.019	0.172

better based on the likelihood ratio (LR) tests for the novel DUSTL_{BHE} model against likely sub-models as reported in Table 6.

The second actual-data is on the glass fibre strength originally reported by [43]. The observations are

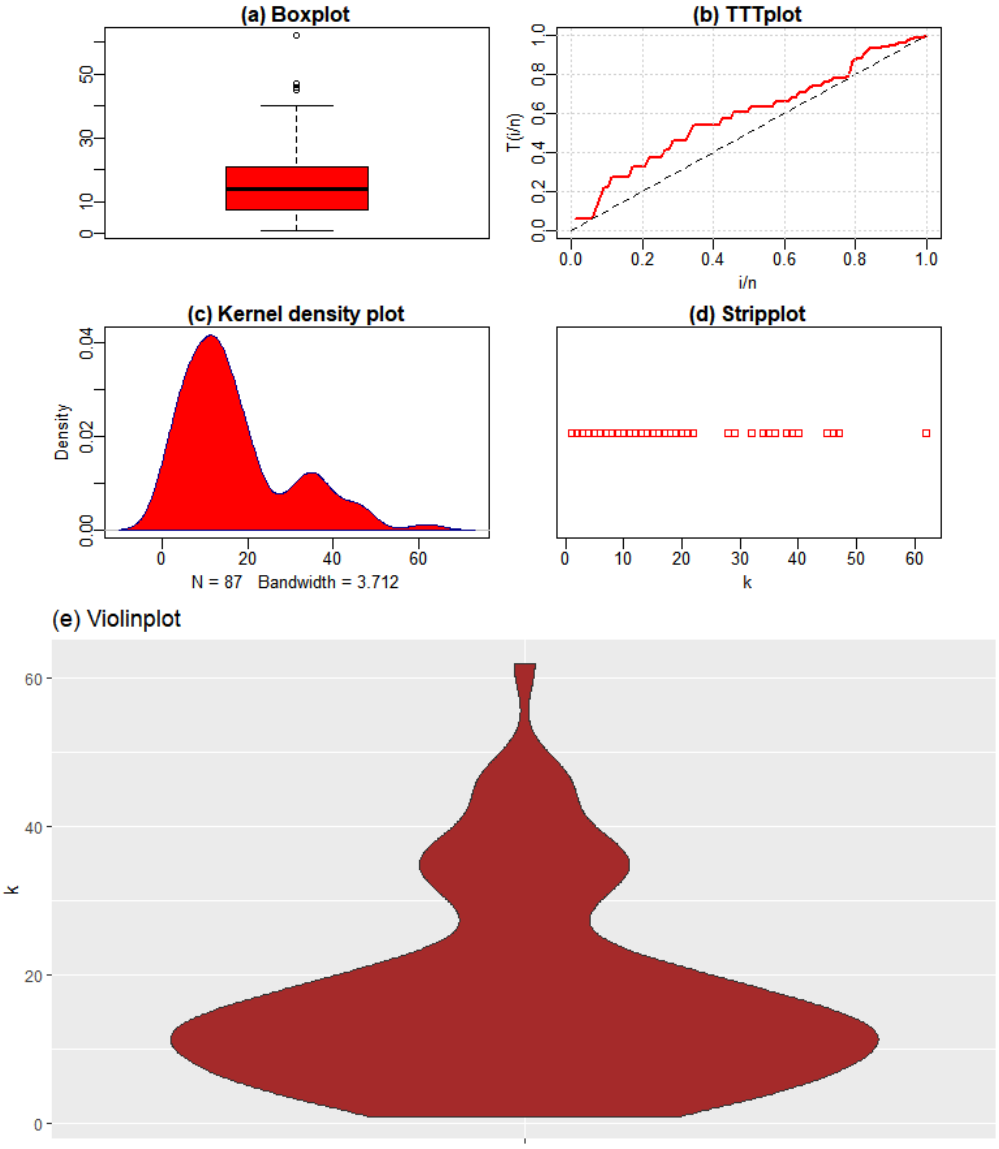

Figure 5. Box-plot, TTT, kernel-density, strip, and violin plots for the first dataset.

Table 5. MLE with performance measures for the first dataset.

Distribution	$\hat{\eta}$	$\hat{\varphi}$	$-\ell$	AIC	BIC	AICc	HQIC	CVMS	ANDL	KSV[KSPV]
DUSTLBHE	1.608 (0.289)	0.027 (0.003)	-328.20	660.40	665.30	660.50	662.40	0.07510	0.5658	0.070 [0.80]
TLBHE	1.846 (0.300)	0.024 (0.003)	-328.70	661.50	666.40	661.60	663.40	0.07715	0.6200	0.080 [0.60]
APE	9.480 (6.291)	0.094 (0.012)	-328.40	660.70	665.70	660.90	662.70	0.10540	0.6715	0.080 [0.60]
BHE	-	0.033 (0.004)	-336.60	675.10	677.60	675.20	676.10	0.07799	0.6135	0.200 [0.01]
APBH	215.753 (67.933)	0.014 (0.006)	-354.00	712.10	717.00	712.20	714.10	0.23271	1.7392	0.300[2E-09]
BH	-	0.002 (0.005)	-454.90	911.90	914.30	911.90	912.90	0.31777	2.3153	0.700[2E-16]
PE	10.641 (5.418)	167.466 (89.048)	-335.30	674.60	679.50	674.70	676.50	0.07615	0.5919	0.200 [0.02]
IPE	3.354 (1.243)	3.008 (1.386)	-345.80	695.70	700.60	695.80	697.60	0.35084	2.5132	0.200 [0.01]
PE1	-	0.401 (0.043)	-383.50	769.00	771.50	769.10	770.00	-	-	0.400[7E-11]
GOM	-6.421 (1.870)	-0.010 (0.003)	-337.20	678.40	683.30	678.50	680.40	0.07598	0.6249	0.200 [0.02]
EIR	0.283 (0.034)	2.204 (0.236)	-372.70	749.50	754.40	749.60	751.50	1.34588	8.2608	0.300[2E-06]
LOMX	9.364 (3.407)	0.007 (0.003)	-335.50	675.00	680.00	675.20	677.00	0.07601	0.5956	0.200 [0.02]
E	-	0.059 (0.006)	-333.40	668.90	671.30	668.90	669.90	0.08135	0.5877	0.200 [0.04]

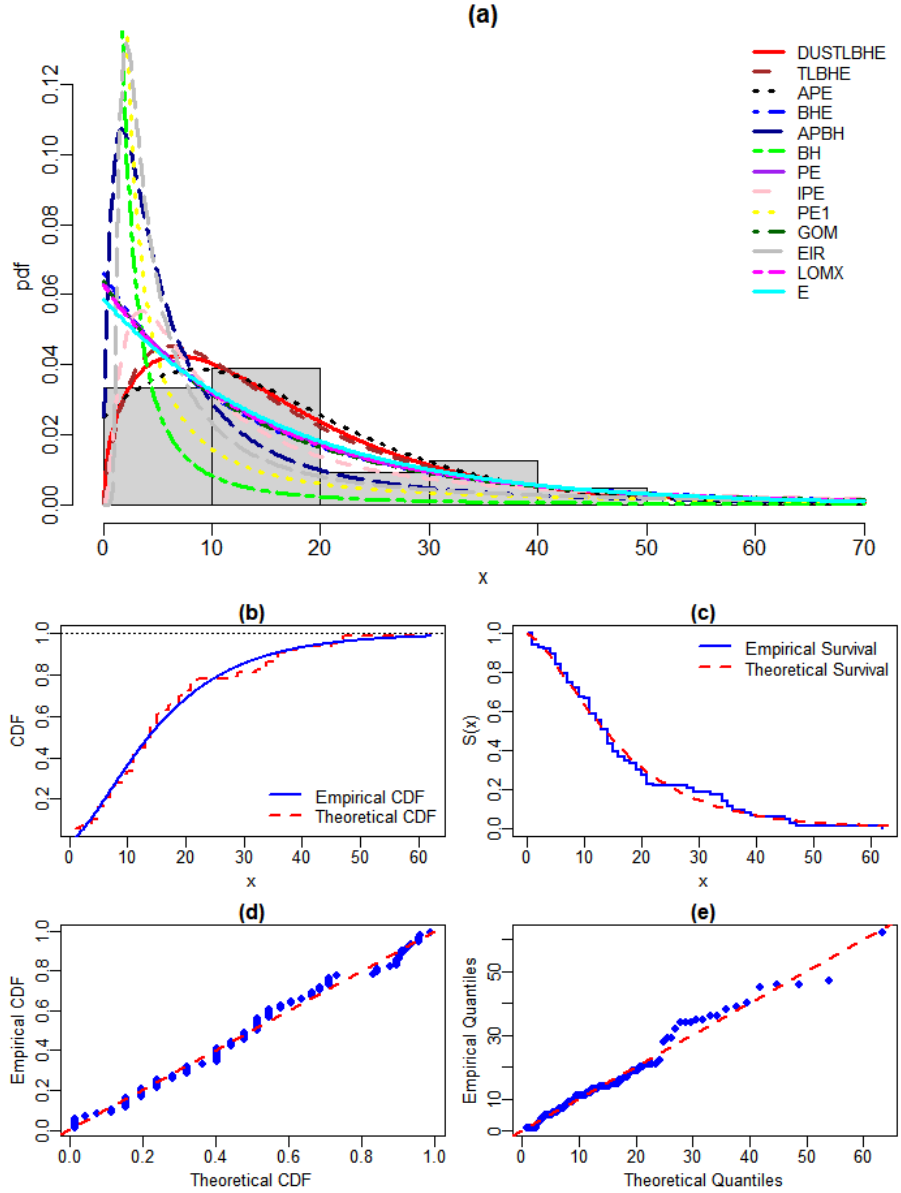

Figure 6. Fitted density functions (pdfs) plot (a), Fitted distribution function (CDF) plot (b), Fitted survival function (CDF) plot (c), P-P plot (d), and Q-Q plot (e) for the DUSTL$_{BHE}$ (first dataset).

Table 6. LR tests for the first dataset

Model	Hypotheses	LR	p-values
DUSTLBHE vs BHE	$H_0 : \eta = 1$ vs $H_1 : H_0$ is false	17	4.3E-05
DUSTLBHE vs BH	$H_0 : \eta = 1$ vs $H_1 : H_0$ is false	253	4.6E-57
DUSTLBHE vs E	$H_0 : \eta = 1$ vs $H_1 : H_0$ is false	10	0.0012

given as follows: 1.014, 1.081, 1.082, 1.185, 1.223, 1.248, 1.267, 1.271, 1.272, 1.275, 1.276, 1.278, 1.286, 1.288, 1.292, 1.304, 1.306, 1.355, 1.361, 1.364, 1.379, 1.409, 1.426, 1.459, 1.460, 1.476, 1.481, 1.484,

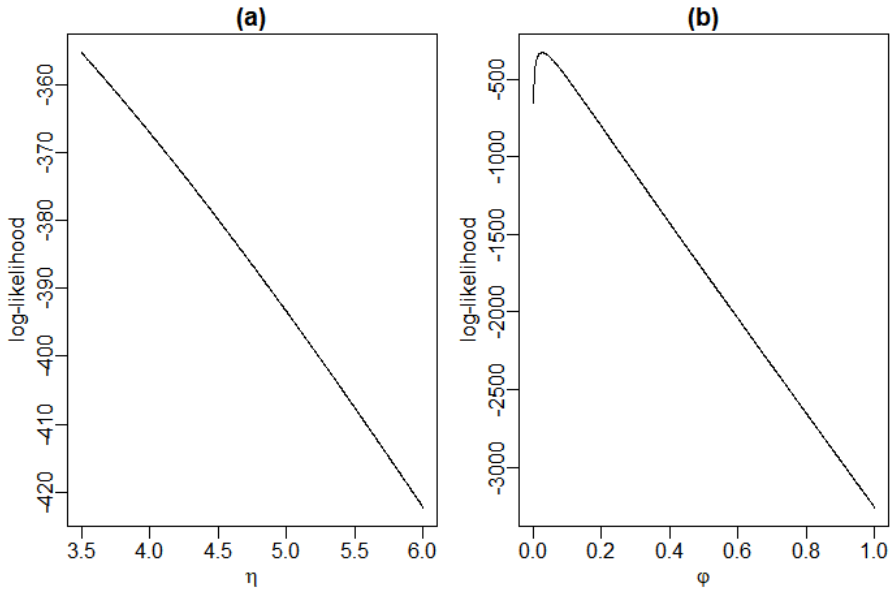

Figure 7. Profile log-likelihood functions for the first dataset.

1.501, 1.506, 1.524, 1.526, 1.535, 1.541, 1.568, 1.579, 1.581, 1.591, 1.593, 1.602, 1.666, 1.670, 1.684, 1.691, 1.704, 1.731, 1.735, 1.747, 1.748, 1.757, 1.800, 1.806, 1.867, 1.876, 1.878, 1.910, 1.916, 1.972, 2.012, 2.456, 2.592, 3.197,4.121. This dataset has been extensively analysed and modeled in the literature, as numerous researchers and scholars have used it to evaluate and compare various statistical distributions. See, [41], [3]. Figures 8 depict the dataset features using the Box-plot, TTT plot, kernel-density plot, and strip plot. The plots confirm the presence of outliers, right-skewness, and increasing failure rate.

Table 7 presents the MLE with standard errors (SEs) and performance measures for the novel DUSTL$_{BHE}$ and the competing distributions. The novel DUSTL$_{BHE}$ has the least values for the performance measures, especially the KSV with high KSPV, confirming the model offers the best fit to the second dataset. Figure 9 depicts clear evidence that the novel DUSTL$_{BHE}$ offers the best fit through the empirical pdf with histogram, empirical cdf, empirical survival, probability-propability (P-P), and quantile-quantile (Q-Q) plots. Figure 10 depicts the log-likelihood profile plots with the estimated MLE parameter values for the second dataset. Furthermore, the empirical findings indicate that the novel model fits the second dataset better based on the likelihood ratio (LR) tests for the novel DUSTL$_{BHE}$ model against likely sub-models as reported in Table 8.

Table 7. MLE with performance measures for the second dataset.

Distribution	$\hat{\eta}$	$\hat{\varphi}$	$-\ell$	AIC	BIC	AICc	HQIC	CVMS	ANDL	KSV[KSPV]
DUSTLBHE	506.294(330.081)	1.486 (0.176)	-22.56	49.12	53.40	49.32	50.80	0.09778	0.7887	0.068 [0.90]
TLBHE	158.479 (67.582)	1.102 (0.111)	-23.06	50.12	54.41	50.32	51.81	0.09927	0.7994	0.120 [0.30]
APE	210.504 (94.628)	1.409 (0.101)	-55.68	115.36	119.64	115.56	117.04	0.28052	1.9649	0.320[3E-06]
BHE	-	0.326 (0.046)	-98.26	198.52	200.66	198.58	199.36	0.27115	1.9038	0.460[6E-13]
APBH	218.336 (90.505)	0.871 (0.098)	-63.32	130.65	134.93	130.85	132.33	0.25293	1.7965	0.370[4E-08]
BH	-	0.232 (0.078)	-113.36	228.73	230.87	228.79	229.57	0.23525	1.6851	0.610[7E-16]
PE	54.283 (53.079)	87.651(86.642)	-93.75	191.50	195.79	191.70	193.19	0.29845	2.0668	0.470[3E-13]
IPE	46.522 (33.250)	0.033 (0.02)4	-93.45	190.90	195.18	191.10	192.58	0.12737	0.9961	0.460[6E-13]
PE1	-	2.233 (0.281)	-40.61	83.22	85.37	83.29	84.07	0.14311	1.0250	0.320[5E-06]
GOM	0.170 (0.056)	1.051 (0.117)	-64.38	132.77	137.05	132.97	134.45	1.18129	6.6991	0.300[2e-05]
EIR	6.753 (1.553)	2.369 (0.128)	-24.03	52.06	56.35	52.26	53.75	0.12636	0.9915	0.097 [0.60]
LOMX	43.934 (29.137)	0.014 (0.009)	-93.87	191.75	196.03	191.95	193.43	0.29704	2.0585	0.470[3E-13]
E	-	0.619 (0.078)	-93.22	188.45	190.59	188.51	189.29	0.30458	2.1029	0.470[2e-13]

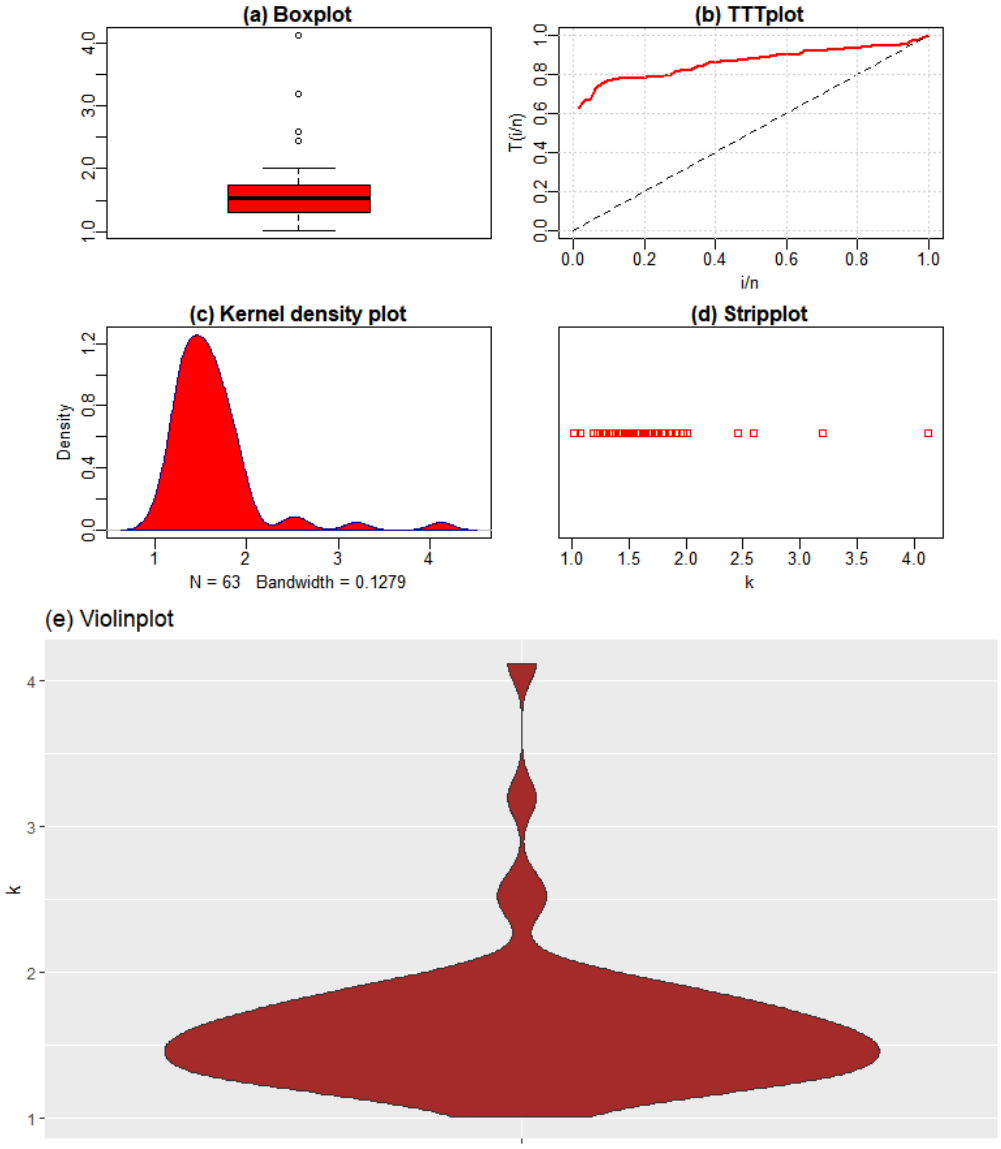

Figure 8. Box-plot, TTT, kernel-density, strip, and violin plots for the second dataset.

Table 8. LR tests for the second dataset

Model	Hypotheses	LR	p-values
DUSTLBHE vs BHE	$H_0 : \eta = 1$ vs $H_1 : H_0$ is false	151	8.6E-35
DUSTLBHE vs BH	$H_0 : \eta = 1$ vs $H_1 : H_0$ is false	182	2.2E-57
DUSTLBHE vs E	$H_0 : \eta = 1$ vs $H_1 : H_0$ is false	141	1.4E-12

The third real dataset pertains to the mortality rates of COVID-19 in Italy, recorded over a 59-day period between 27th February and 27th April 2020, as reported by [7]. The recorded mortality rate observations are as follows: 4.571, 7.201, 3.606, 8.479, 11.410, 8.961, 10.919, 10.908, 6.503, 18.474, 11.010, 17.337, 16.561, 13.226, 15.137, 8.697, 15.787, 13.333, 11.822, 14.242, 11.273, 14.330, 16.046, 11.950, 10.282,

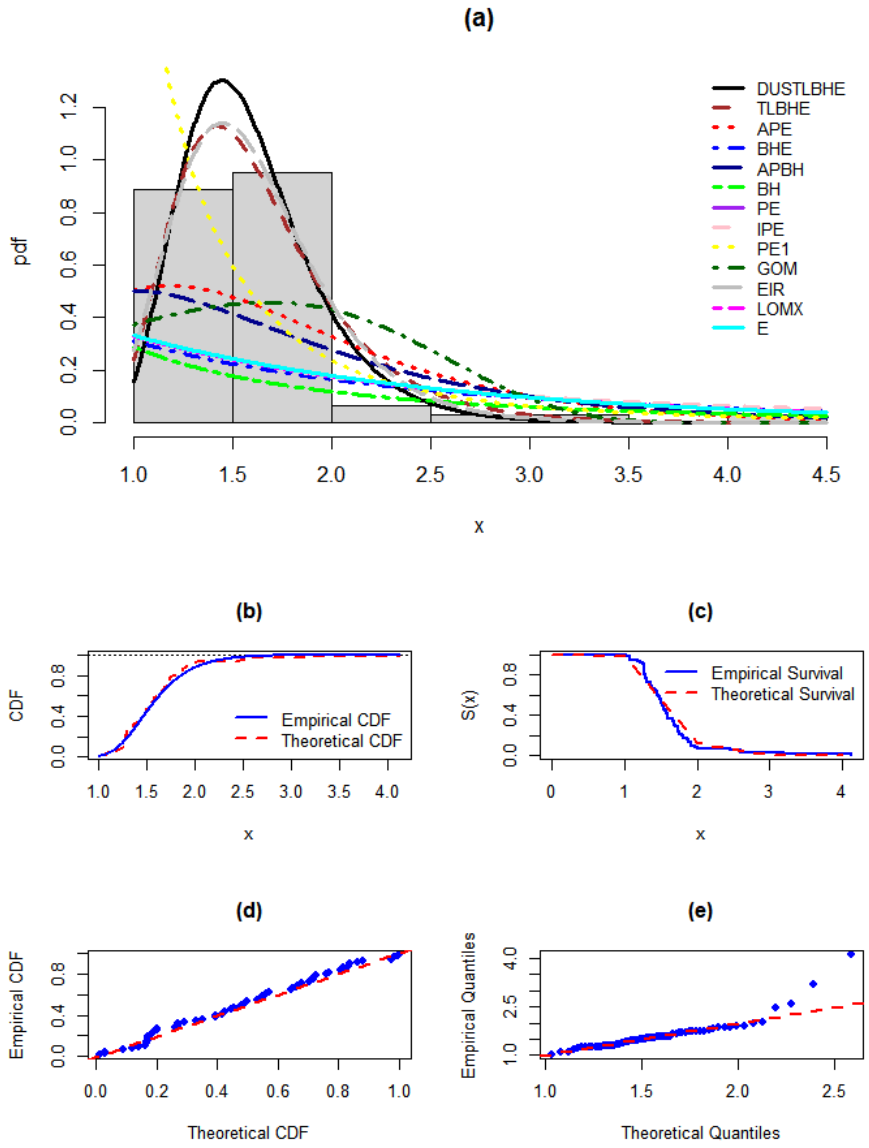

Figure 9. Fitted density functions (pdfs) plot (a), Fitted distribution function (CDF) plot (b), Fitted survival function (CDF) plot (c), P-P plot (d), and Q-Q plot (e) for the DUSTL$_{BHE}$ (second dataset).

11.775, 10.138, 9.037, 12.396, 10.644, 8.646, 8.905, 8.906, 7.407, 7.445, 7.214, 6.194, 4.640, 5.452, 5.073, 4.416, 4.859, 4.408, 4.639, 3.148, 4.040, 4.253, 4.011, 3.564, 3.827, 3.134, 2.780, 2.881, 3.341, 2.686, 2.814, 2.508, 2.450, 1.518. This dataset reflects the daily progression of COVID-19-related deaths during the early stages of the pandemic in Italy and has been used to evaluate the performance of probabilistic models in epidemiological analysis. See, [36, 35]. Figures 11 depict the dataset features using the Box-plot, TTT plot, kernel-density plot, and strip plot. The plots confirm the presence of no outliers, right-skewness, and increasing failure rate.

Table 9 presents the MLE with standard errors (SEs) and performance measures for the novel DUSTL$_{BHE}$

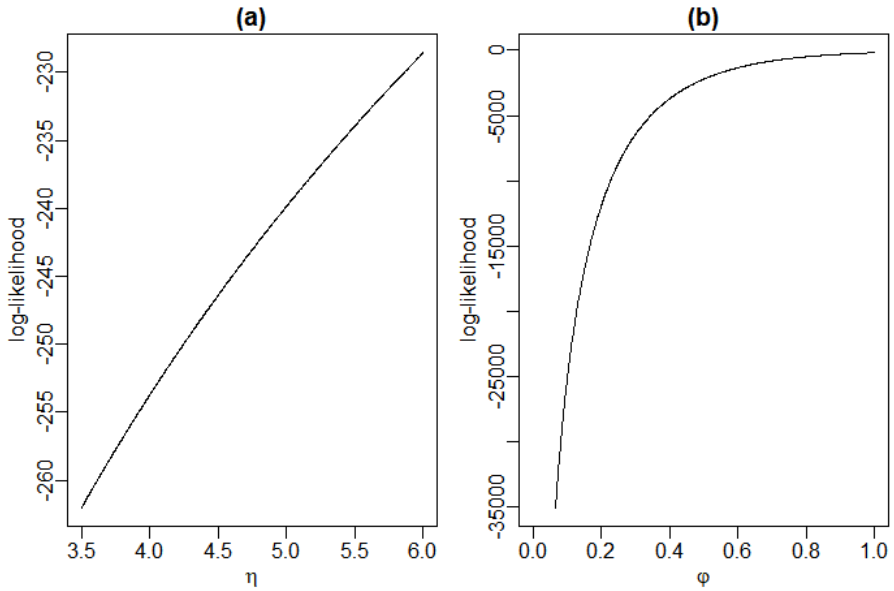

Figure 10. Profile log-likelihood functions for the second dataset.

and the competing distributions. The novel DUSTL$_{BHE}$ has the least values for the performance measures, especially the KSV with high KSPV, confirming the model offers the best fit to the third dataset. Figure 12 depicts clear evidence that the novel DUSTL$_{BHE}$ offers the best fit through the empirical pdf with histogram, empirical cdf, empirical survival, probability-probability (P-P), and quantile-quantile (Q-Q) plots. Figure 13 depicts the log-likelihood profile plots with the estimated MLE parameter values for the third dataset. Furthermore, the empirical findings indicate that the novel model fits the third dataset better based on the likelihood ratio (LR) tests for the novel DUSTL$_{BHE}$ model against likely sub-models as reported in Table 10.

Table 9. MLE with performance measures for the third dataset.

Distribution	$\hat{\eta}$	$\hat{\varphi}$	$-\ell$	AIC	BIC	AICc	HQIC	CVMS	ANDL	KSV [KSPV]
DUSTLBHE	3.824 (1.018)	0.083 (0.012)	-168.3	340.6	344.8	340.8	342.2	0.1625	0.9281	0.112 [0.41]
TLBHE	4.197 (1.015)	0.074 (0.011)	-168.4	340.8	344.9	341.0	342.4	0.1692	0.9565	0.114 [0.40]
APE	62.460 (46.060)	0.251 (0.027)	-169.5	343.1	347.2	343.3	344.7	0.1643	0.9719	0.113 [0.40]
BHE	-	0.067 (0.010)	-186.2	374.5	376.6	374.6	375.3	0.1650	0.9825	0.254 [0.00]
APBH	921.600 (457.000)	0.080 (0.019)	-177.0	358.1	362.2	358.3	359.7	0.1711	0.9619	0.185 [0.03]
BH	-	0.011 0.015	-245.6	493.2	495.3	493.3	494.0	0.1895	1.0668	0.701 [7.8E-16]
PE	13.080 (7.486)	103.000 (61.060)	-184.4	372.8	376.9	373.0	374.4	0.1632	0.9757	0.248 [0.00]
IPE	37.190 (31.010)	0.153 (0.130)	-184.6	373.2	377.3	373.4	374.8	0.2282	1.3043	0.264 [0.00]
PE1	-	0.519 (0.068)	-211.3	424.5	426.6	424.6	425.3	0.2290	1.3381	0.355 [3.5E-07]
GOM	0.296 (0.126)	0.151 (0.028)	-169.6	343.2	347.3	343.4	344.8	0.1626	0.9419	0.113 [0.40]
EIR	0.788 (0.132)	4.318 (0.402)	-175.5	355.0	359.1	355.2	356.6	0.2882	1.6951	0.179 [0.04]
LOMX	20.980 (9.577)	0.006 (0.003)	-183.8	371.6	375.8	371.8	373.2	0.1662	0.9658	0.245 [0.00]
E	-	0.123 (0.016)	-182.8	367.7	369.7	367.7	368.5	0.1678	0.9490	0.242 [0.00]

Table 10. LR tests for the third dataset

Model	Hypotheses	LR	p-values
DUSTLBHE vs BHE	$H_0 : \eta = 1$ vs $H_1 : H_0$ is false	36	2.1E-09
DUSTLBHE vs BH	$H_0 : \eta = 1$ vs $H_1 : H_0$ is false	155	1.7E-35
DUSTLBHE vs E	$H_0 : \eta = 1$ vs $H_1 : H_0$ is false	29	7.1E-08

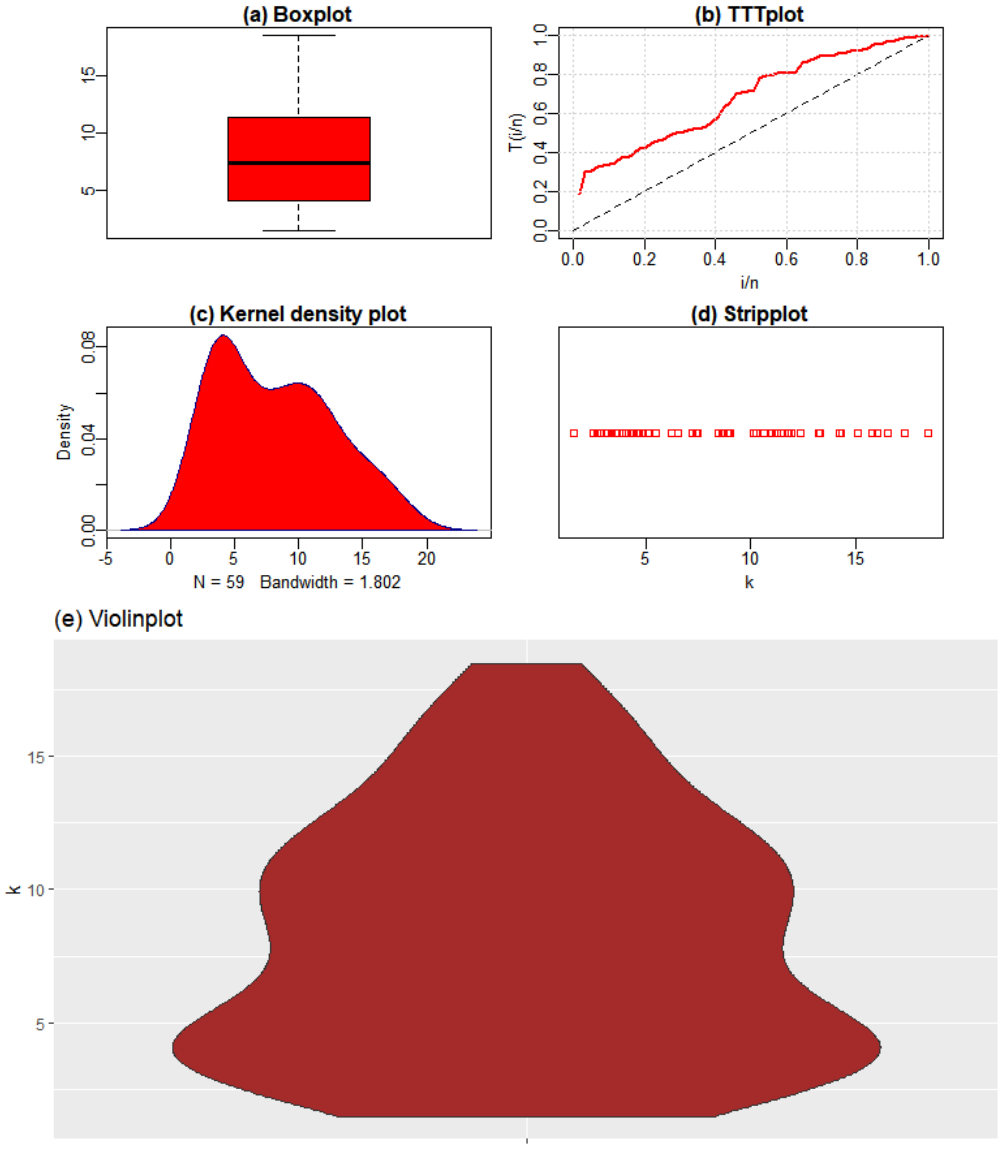

Figure 11. Box-plot, TTT, kernel-density, strip, and violin plots for the third dataset.

The large parameter estimates in Tables 5, 7, and 9 arise due to the scaling characteristics of the datasets and the flexibility of the proposed distribution. In particular, the likelihood surface may produce large estimates when the datasets exhibit strong skewness or heavy-tailed behaviour. Additionally, the optimization procedure converges properly, and the estimates correspond to valid maximum likelihood solutions.

7. Conclusion

This study proposed a new flexible probability distribution known as the DUS-Topp-Leone Burr-Hatke-Exponential (DUSTL$_{BHE}$) distribution. The developed model exhibits greater flexibility and wider applicability than the BHE model and several other well-known statistical models, particularly in the medical and engineering sciences. Several important statistical properties of the DUSTL$_{BHE}$ distribution were derived,

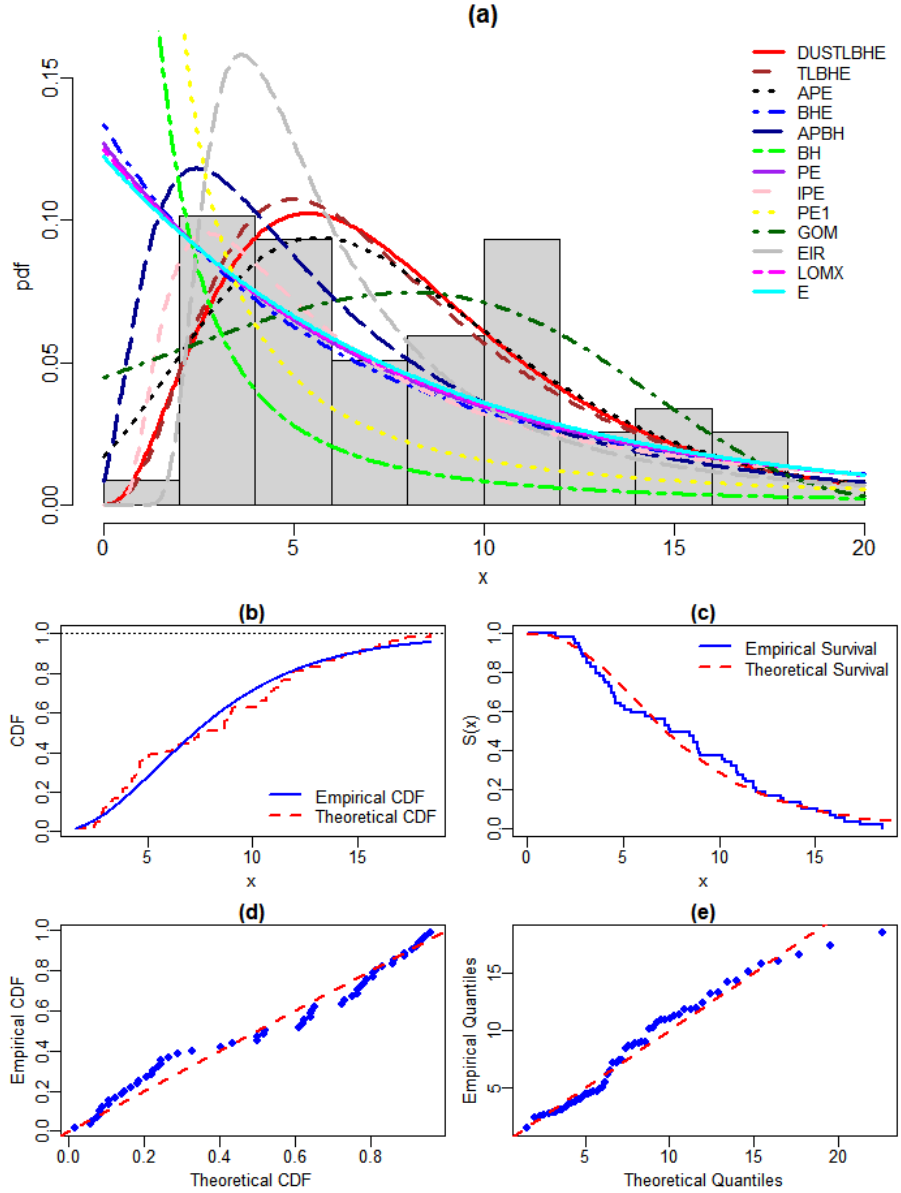

Figure 12. Fitted density functions (pdfs) plot (a), Fitted distribution function (CDF) plot (b), Fitted survival function (CDF) plot (c), P-P plot (d), and Q-Q plot (e) for the DUSTL$_{BHE}$ (third dataset).

including the density function, distribution function, linear representation, asymptotic behaviour, moments, MGF, and others. Parameter estimation for the model was performed using the maximum likelihood estimation (MLE) method, and a simulation study was conducted to assess the accuracy and efficiency of the MLE. The usefulness of the new model was illustrated through applications to three real-world datasets from the medical and engineering domains. The results from the empirical analysis show that the DUSTL$_{BHE}$ distribution provides better goodness-of-fit performance compared with several competing models according to standard model selection criteria such as the log-likelihood, AIC, BIC, and others. This indicates that the DUSTL$_{BHE}$ distribution is capable of effectively capturing complex data characteristics such as strong

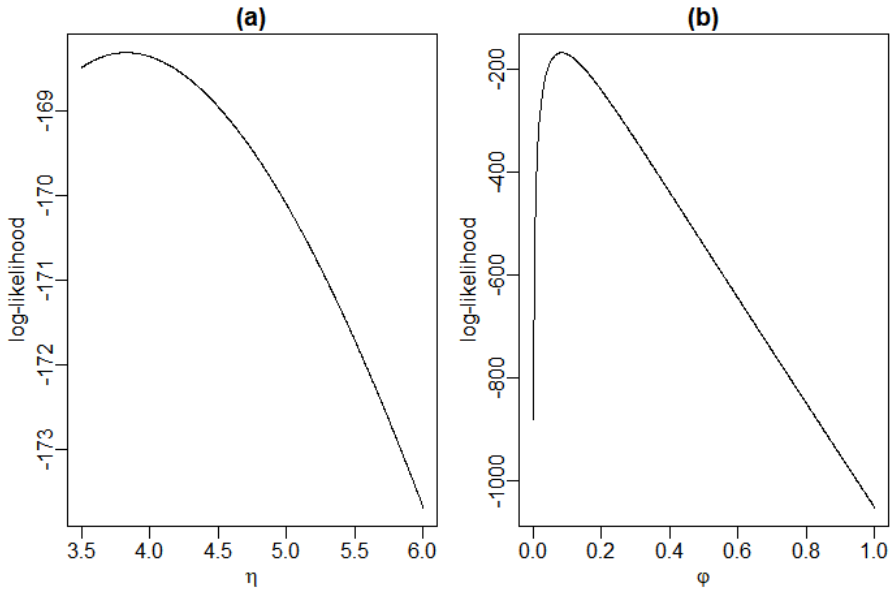

Figure 13. Profile log-likelihood functions for the third dataset.

skewness and heavy tails. The flexibility of the proposed model makes it a promising tool for analysing lifetime and reliability data arising in epidemiology, public health studies, actuarial science and engineering reliability analysis. Future research may explore several extensions of the proposed distribution. These include the development of regression models based on the DUSTL$_{BHE}$ distribution, Bayesian estimation procedures, multivariate extensions, and applications in survival analysis and reliability modelling. In addition, simulation studies could be conducted to further investigate the statistical properties and efficiency of the parameter estimators under different sampling conditions.

Authors' Contributions

Conceptualization, O.D.A and U.F.A; Methodology, O.D.A and U.F.A; Software, O.D.A.; Validation, O.D.A and U.F.A; Formal Analysis, O.D.A.; Investigation, O.D.A and U.F.A; Resources, O.D.A and U.F.A; Data Curation, O.D.A and U.F.A; Writing – Original Draft Preparation, O.D.A; Writing – Review & Editing, O.D.A and U.F.A; Visualization, O.D,A.; Supervision, O.D.A and U.F.A; Project Administration, O.D.A and U.F.A; Funding Acquisition, O.D.A and U.F.A).

Data Availability Statement

The data used can be found within the manuscript.

Conflicts of Interest

The authors declare no conflict of interest in this study.

Acknowledgments

We acknowledge the management of Federal University Wukari and Gombe State Polytechnic for providing a suitable environment for the conceptualization and finalization of this study.

References

1.Abdulkadir, A., Adubisi, O. D., and Madaki, R. (2024). A new family of distributions based on amalgamation of two methods with an application to the Rayleigh model. *European Journal of Statistics*, 4:1–19.

2.Abramowitz, M. and Stegun, I. A. (1972). *Handbook of Mathematical Functions with Formulas, Graphs, and Mathematical Tables*. Dover Publications, New York.

3.Adubisi, O. D. (2026). A new generated lifetime model: theory, simulation and applications to stress-strength datasets. *Iraqi Statistician Journal*, 3:33–45.

4.Adubisi, O. D., Joshua, J., and David, A. A. (2025). Alpha-power burr–hatke exponential model: Properties, simulations and applications based on uncensored and progressive type-ii censored samples. *Journal of Reliability Theory and Application*, 20(3):455–472.

5.Akkanphudit, T., Bodhisuwan, W., Lao, M., and Volodin, A. (2020). The Topp–Leone discrete Laplace distribution and its applications. *Lobachevskii Journal of Mathematics*, 41:298–307.

6.Alghamdi, A. S. and Abd El-Raouf, M. (2023). Exploring the dynamics of COVID-19 with a novel family of models. *Mathematics*, 11:1641.

7.Almongy, H. M., Almetwally, E. M., Aljohani, H. M., Alghamdi, A. S., and Hafez, E. (2021). A new extended Rayleigh distribution with applications to COVID-19 data. *Results in Physics*, 23:104012.

8.Alyami, M. H., Naser, A. Y., Orabi, M. A. A., Alwafi, H., and Alyami, H. S. (2020). Epidemiology of COVID-19 in the Kingdom of Saudi Arabia: An ecological study. *Frontiers in Public Health*, 8:506.

9.Alyami, S. A., Elbatal, I., Alotaibi, N., Almetwally, E. M., Okasha, H. M., and Elgarhy, M. (2022). Topp–Leone modified Weibull model: Theory and applications to medical and engineering data. *Applied Sciences*, 12:10431.

10.Anyiam, K. E., Alghamdi, F. M., Nwaigwe, C. C., Aljohani, H. M., and Obulezi, O. J. (2024). A new extension of the Burr–Hatke exponential distribution with engineering and biomedical applications. *Heliyon*, 10(19):e38293.

11.Arimoto, S. (1971). Information-theoretical considerations on estimation problems. *Information and Control*, 19:181–194.

12.Arnold, B. C. (2015). *Pareto Distributions*. CRC Press, New York.

13.Astorga, J. M. and Iriarte, Y. A. (2025). Lambert–Topp–Leone distribution: An alternative for modeling proportion and lifetime data. *Frontiers in Applied Mathematics and Statistics*, 11:1527833.

14.Atchade, M. N., N'bouké, M. A. G., Djibril, A. M., Al-Mutairi, A., Mustafa, M. S., Hussam, E., Alsuhabi, H., and Nassr, S. (2024). A new Topp–Leone Kumaraswamy Marshall–Olkin generated family of distributions with applications. *Heliyon*, 10:e24001.

15.Badmus, N. I., Faweya, O., and Ige, S. A. (2023). Parametric modeling approach to COVID-19 pandemic data. *Open Journal of Statistics*, 13:61–73.

16.Balakrishnan, N. and Basu, A. P. (1995). *The Exponential Distribution: Theory, Methods and Applications*. Gordon and Breach, Newark.

17.Bantan, R. A. R., Jamal, F., Chesneau, C., and Elgarhy, M. (2019). A new power Topp–Leone generated family of distributions with applications. *Entropy*, 21:1177.

18.Chipepa, F., Oluyede, B., and Makubate, B. (2024). The Topp–Leone Marshall–Olkin-G family of distributions with applications. *International Journal of Statistics and Probability*, 9:15–32.

19.Corless, R. M. (1996). On the Lambert W function. *Advances in Computational Mathematics*, 5:329–359.

20.Ekemezie, D. F. N., Anyiam, K. E., Kayid, M., Balogun, O. S., and Obulezi, O. J. (2024). DUS Topp–Leone-G family of distributions: Baseline extension, properties, estimation, simulation and applications. *Entropy*, 26:973.

21.Eliwa, M. S., Alhumaidan, B. T., and Alqefari, R. N. (2023). A discrete mixed distribution: Statistical and reliability properties with applications to model COVID-19 data in various countries. *Mathematical Biosciences and Engineering*, 20:7859–7881.

22.Gompertz, B. (1825). On the nature of the function expressive of the law of human mortality and on a new mode of determining the value of life contingencies. *Philosophical Transactions of the Royal Society of London*, 115:513–583.

23.Gradshteyn, I. S. and Ryzhik, I. M. (2014). *Table of Integrals, Series, and Products*. Academic Press, Amsterdam, 8 edition.

24.Hassan, E. A. A., Elgarhy, M., Eldessouky, E. A., Hassan, O. H. M., Amin, E. A., and Almetwally, E. M. (2023). Different estimation methods for new probability distribution approach based on environmental and medical data. *Axioms*, 12:220.

25.Havrda, J. and Charvát, F. (1967). Quantification method of classification processes: Concept of structural α-entropy. *Kybernetika*, 3:30–35.

26.Isaic-Maniu, A. and Vodă, V. G. (2008). Generalized Burr–Hatke equation as generator of a homographic failure rate. *Journal of Applied Quantitative Methods*, 3:3.

27.Johnson, N. L., Kotz, S., and Balakrishnan, N. (1994). *Continuous Univariate Distributions*, volume 1. John Wiley & Sons, New York, 2 edition.

28.Klugman, S. A., Panjer, H. H., and Willmot, G. E. (2019). Loss models: from data to decisions.

29.Liu, P. and Zheng, Y. (2023). Heavy-tailed distributions of confirmed COVID-19 cases and deaths in spatiotemporal space. *PLoS ONE*, 18:e0294445.

30.Lomax, K. S. (1954). Business failures: Another example of the analysis of failure data. *Journal of the American Statistical Association*, 49:847–852.

31.Mahdavi, A. and Kundu, D. (2017). A new method for generating distributions with an application to exponential distribution. *Communications in Statistics – Theory and Methods*, 46(13):6543–6557.

32.Nanga, S., Nasiru, S., and Dioggban, J. (2022). Tangent Topp–Leone family of distributions. *Scientific African*, 17:e01363.

33.Nanga, S., Nasiru, S., and Dioggban, J. (2023). Cosine Topp–Leone family of distributions: Properties and regression. *Research in Mathematics*, 10.

34.Parashar, L., Shekhar, H., Arya, H., Vig, S. L., and Prasad, J. (2025). Statistical probability distribution for the COVID-19 mortality rate. *Journal of Information Systems Engineering and Management*, 10:64–75.

35.Pavitra, K. and Vinay, D. (2024). Statistical properties and applications of the modified exponential inverse Lindley distribution. *Heliyon*, 10:e25438.

36.Qayoom, D., Rather, A. A., Alotaibi, E. S., Shukr, B. A., Almazmomi, A. A., and Alshammari, A. O. (2025). A novel extension of the power Lindley distribution with statistical properties and application to COVID-19 data. *Scientific Reports*, 15:30486.

37.Rao, G. S. and Mbwambo, S. (2019). Exponentiated inverse rayleigh distribution and an application to coating weights of iron sheets data. *Journal of Probability and Statistics*, 19(1):7519429.

38.Rényi, A. (1961). On measures of information and entropy. *Proceedings of the Fourth Berkeley Symposium on Mathematical Statistics and Probability*, pages 547–561.

39.Reyad, H. M., Alizadeh, M., Jamal, F., Othman, S., and Hamedani, G. G. (2019). The exponentiated generalized Topp–Leone-G family of distributions: Properties and applications. *Pakistan Journal of Statistics and Operation Research*, 15:1–24.

40.Rezaei, S., Sadr, B. B., Alizadeh, M., and Nadarajah, S. (2016). Power Topp–Leone generated family of distributions: Properties and applications. *Communications in Statistics–Theory and Methods*, 46:2893–2909.

41.Shalabi, L. A. (2021). The Topp–Leone Weibull distribution: Properties and applications. *Journal of Statistical Applications and Probability*, 9:237–247.

42.Shannon, C. E. (1948). A mathematical theory of communication. *Bell System Technical Journal*, 27:379–423.

43.Smith, R. L. and Naylor, J. C. (1987). A comparison of maximum likelihood and Bayesian estimators for the three-parameter Weibull distribution. *Applied Statistics*, 36:358–369.

44.Sule, I., Doguwa, S., Isah, A., and Jibril, H. (2020a). On the Topp–Leone exponentiated-G family of distributions: Properties and applications. *Asian Journal of Probability and Statistics*, 7:1–15.

45.Sule, I., Doguwa, S., Isah, A., and Jibril, H. (2020b). The Topp–Leone Kumaraswamy-G family of distributions with applications to cancer disease data. *Journal of Biostatistics and Epidemiology*, 6:40–51.

46.Tashkandy, Y., Almetwally, E. M., and Alqurashi, A. (2023). The transmuted odd Fréchet–Lomax distribution: Properties and applications. *Computational and Mathematical Methods*, 5:e1265.

47.Topp, C. W. and Leone, F. C. (1955). A family of J-shaped frequency functions. *Journal of the American Statistical Association*, 50(269):209–219.

48.Tsallis, C. (1988). Possible generalization of Boltzmann–Gibbs statistics. *Journal of Statistical Physics*, 52:479–487.

49.Yadav, A. S., Altun, E., and Yousof, H. M. (2021). Burr–hatke exponential distribution: A decreasing failure rate model, statistical inference and applications. *Annals of Data Science*, 8(2):241–260.

50.Yousof, H. M., Alizadeh, M., Jahanshahi, S. M. A., Ramires, T. G., Ghosh, I., and Hamedani, G. G. (2017). The transmuted Topp–Leone-G family of distributions: Theory, characterizations and applications. *Journal of Data Science*, 15:723–740.